Materials & Design 218 (2022) 110711

Contents lists available at ScienceDirect

Materials & Design

journal homepage: www.elsevier.com/locate/matdes

Fabrication and characterization of double-layer asymmetric dressing through electrostatic spinning and 3D printing for skin wound repair

Ting Zhang [a], Hao Xu [a], Yonggang Zhang [a,b], Siruo Zhang [c], Xia Yang [c], Yan Wei [a,b], Di Huang [a,b], Xiaojie Lian [a,b,*]

[a] Department of Biomedical Engineering, Research Center for Nano-biomaterials and Regenerative Medicine, College of Biomedical Engineering, Taiyuan University of Technology, Taiyuan 030024, PR China
[b] Shanxi Key Laboratory of Material Strength & Structural Impact, Institute of Biomedical Engineering, Taiyuan University of Technology, Taiyuan 030024, PR China
[c] Shanxi Provincial Key Laboratory for Functional Proteins, Shanxi Jinbo Bio-Pharmaceutical Co., Ltd, Taiyuan 030032, PR China

HIGHLIGHTS

- A bilayer asymmetric dressing was developed to mimic the gradient structure of epidermis and dermis.
- The dense outer layer with better water repellency was made of PCL/PLA by electrostatic spinning.
- The porous inner layer with water absorbing capacity was made of SA/PVA adding HACC by 3D printing.
- The bilayer asymmetric dressing has similar mechanical properties to natural human skin.

GRAPHICAL ABSTRACT

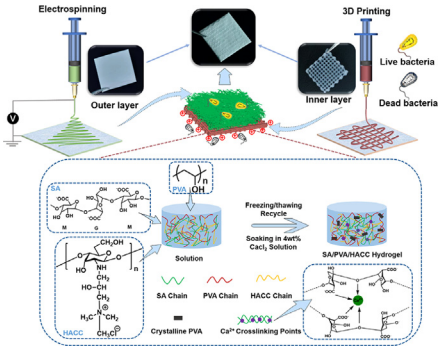

ARTICLE INFO

Article history:
Received 15 January 2022
Revised 26 April 2022
Accepted 28 April 2022
Available online 4 May 2022

Keywords:
Electrostatic spinning
3D printing
Hydrogel
Wound dressing
Antibacterial property

ABSTRACT

Ideal wound dressings provide optimal microenvironment for the reconstruction of damaged tissue. In this work, we fabricated a bilayer asymmetric dressing to mimic gradient structure of epidermis and dermis of skin by combining electrostatic spinning and 3D printing method with properties including surface hydrophilic and hydrophobic, porosity, mechanical as well as antibacterial properties. The outer layer was prepared by optimized PCL/PLA (PP) via electrostatic spinning to mimick epidermis with water repellency and against bacterial penetration, which has a tensile modulus of 19.69 ± 0.66 MPa. While, the inner layer was 3D printed by optimized sodium alginate/polyvinyl alcohol/chitosan quaternary ammonium salt (SPH). The tensile modulus of SPH with a porosity of 70–90% is 0.82 ± 0.01 MPa, and the water content can be achieved above 85%. The antibacterial efficacy of inner layer was tested against *Staphylococcus aureus* indicating forming inhibition zone with a diameter of 1.61 ± 0.35 cm. In addition, Cell Counting Kit-8 and Live/Dead assay was used to test the viability of human dermal fibroblasts (HFBS), which showed that PP/SPH with 6% PVA had not significant cytotoxic effects. The double-layer asymmetric dressing meets the requirements of skin mechanical properties and provides an effective repair strategy for clinical skin trauma.

* Corresponding author at: Department of Biomedical Engineering, Research Center for Nano-biomaterials and Regenerative Medicine, College of Biomedical Engineering, Taiyuan University of Technology, Taiyuan 030024, PR China.
E-mail address: yuhalian@126.com (X. Lian).

https://doi.org/10.1016/j.matdes.2022.110711
0264-1275/

1. Introduction

The skin is the body's first defense barrier from external circumstances [1]. After the occurrence of a skin injury, to avoid further infection, a skin substitute is needed to protect the underlying tissues and prevent the loss of body fluids [2,3]. Wound dressing is a covering or a protective layer for wounds, which can provide temporary protection and control wound infection during wound healing, providing a suitable healing environment on the traumatized surface [4]. Trauma dressings are divided into traditional dressings [5], biological dressings [6], synthetic dressings [7] and growth factor dressings [8,9] depending on their different materials. Depending on the complexity of the wound, wound dressings have been designed in different forms and properties, including closure dressings, non-bonded dressings, absorbent dressings and dressings in the form of sheets, foams, powders and gels [10]. Although some dressings are cheap and readily available, they usually have disadvantages such as poor affinity to the wound area and insufficient water vapor permeability, leading to exudate accumulation, tissue maceration or the development of infection [11]. Ideal wound dressings are often derived from natural materials with skin-like properties, should adhere closely to the injured tissue, maintain water balance, allow gas exchange, and absorb secretions, support cell proliferation, mechanical compatibility, and inhibit bacterial growth, thus ensuring an optimal microenvironment to improve wound healing to a more humanistic level [12,13,14,15].

Therefore, asymmetric membrane has attracted the attention of researchers in recent years because of their flexible design for similarity to the natural skin structure. Asymmetric membranes are usually composed of a dense outer layer and a porous inner layer, similar to the epidermal and enderonic layer of the skin. The dense outer layer protects the wound tissue from external threats (physical, chemical agents and bacteria) and controls gas exchange (water vapor, O_2 or CO_2) [16]. On the other hand, the inner layer with a porous structure can absorb exudates and support cell adhesion and proliferation [17,18]. Moreover, asymmetric membranes can be fabricated using multiple techniques such as wet, dry/wet phase inversion, $scCO_2$-assisted phase inversion, electrostatic spinning, and 3D printing [19].

Meanwhile, there are a variety of materials used for skin repair. Polycaprolactone (PCL) has been widely used to promote skin tissue regeneration or trauma dressings because of its high mechanical flexibility, inherent non-toxicity, low biodegradability, high biocompatibility, and high ECM mimicry [20]. In addition, the low hydrophilicity of PCL makes it a unique biopolymer used to mimic the skin surface and act as a hydrophobic barrier [21]. However, Soft PCL's modulus is nearly one order of magnitude lower than that of PLA, so polylactic acid (PLA) with excellent mechanical properties is introduced to meet the needs in other study [22,23]. PLA is a semi-crystalline thermoplastic polymer with relatively high modulus of elasticity and brittle, low elongation [24]. PLA/PCL composite have good synergistic and complementary properties, and by adjusting the ratio of PLA and PCL, making for the improvement on mechanical properties of the composite [25]. There are research on PLA/PCL electrostatic spinning film used for skin regeneration but is rarely reported to conbine 3D printed porous layer simultaneously improving water absorption, as well as antibacterial properties [26,27].

Sodium alginate (SA) is a natural polymer that is widely used in 3D printed tissue regeneration to construct a porous structure [28]. It has high biocompatibility, low toxicity and excellent rheological properties [29]. Furthermore, SA has a water absorption capacity of 20–30 times its weight and releases encapsulated drugs and molecules when in contact with moist environments, and can absorb wound secretions due to its high water absorption properties [30,31]. But the printability of SA needs to be improved by adding some biopolymers. There are some study on SA/PVA skin substitute [32]. Polyvinyl alcohol (PVA) has good hydrophilic and biocompatible properties, as well as adjustable mechanical properties suitable for dressings, and can be crosslinked by being frozen and thawed at low temperature without the addition of any chemical agent to make PVA molecules tightly bound by van der Waals forces [33,34,35]. In order to prevent skin infection, chitosan quaternary ammonium salt (HACC) can be used as antibacterial agent. HACC is a natural quick-water-soluble cationic polysaccharide, which is an advanced derivative of chitosan made by chemical modification of marine chitosan [36]. The antimicrobial performance of HACC is better than chitosan and other chitosan derivatives [37].

Herein, a novel asymmetric membrane was developed to mimic the gradient structure of epidermis and dermis of natural skin combining electrostatic spinning and 3D printing technology for wound dressing in this study. Furthermore, the fabrication of two layers of gradient material structure takes into account the differences in physiological functions mainly performed by the epidermis and dermis, such as the surface hydrophilic and hydrophobic, pore structure, mechanical property as well as the requirements to promote skin cell growth. To be specific, a dense electrostatic spinning membrane with better mechanical property and water repellency was made of optimized PCL/PLA as a protective barrier against microbial penetration, which was served as the epidermal layer of the skin. For dermis layer, the porous 3D printed construct with water absorbing capacity was designed to provide an antibacterial environment for wound healing, which is printed by optimized SA/PVA adding HACC. The complementarity of gradient material properties and structure would achieve an optimal microenvironment to accelerate the healing process. As a whole, this study would provide an enhanced material design strategy for future clinical skin wound repair.

2. Materials and methods

2.1. Materials

N, N-dimethylformamide (DMF) and dichloromethane (DCM) were purchased from Shanghai Titan Scientific Co., Ltd, China. The polycaprolactone (PCL) (Mw: 80,000) were purchased from Shanghai Yuanye Bio-Technology Co., Ltd, China and polylactic acid (PLA) (Mw: 44,000) were obtained from Kooer Biotech Co., Ltd, China. Sodium alginate (SA) (viscosity: 200–500 mp·s) was purchased from Shanghai Yien Chemical Technology Co., Ltd, China. Polyvinyl alcohol (PVA-124) (viscosity: 54–66 mp·s) was obtained from Xilong Scientific Co., Ltd, China. And Chitosan quaternary ammonium salt (HACC) has been obtained from MackLin, China. All other chemicals and reagents used were of analytical grade.

2.2. Methods

2.2.1. The preparation of electrostatic spinning film

A blend solution of 12% PCL (w/v) and 6% PLA (w/v) was prepared by dissolving in a 7:3 (v/v) ratio mixture of DCM and DMF. Afterwards, the solution was placed in a special syringe (20 mL) and electrospun at a constant flow rate of 0.003 mm/s under KH-1089 electrostatic spinning equipment with spinning needle (21G), at 25 °C (humidity of 25%), using a working distance of 18 cm. Meanwhile, PCL/PLA electrostatic spinning nanofiber film was obtained at a drum speed of 300 r/min and an applied voltage of 24 kV.

2.2.2. Preparation of inner 3D printed hydrogels

The 6% of PVA (w/v) was dissolved in 20 mL of deionized water, and placed in a magnetic stirrer at 92 °C until PVA was completely dissolved. After PVA solution was naturally cooled to room temperature (25 °C), 1% HACC (w/v) powders were added, and then stirred magnetically at 25 °C until the HACC was completely dissolved. Increasing the temperature to 45 °C, 5% SA (w/v) was slowly added and dissolved in the solution to obtain the 3D printing ink. The materials were all printed using a bio-3D printer (SunP BioMaker 1) at an ambient temperature of 25 °C, humidity of 40%. The obtained SA/PVA/HACC bioink was placed in a special syringe (BD-5 mL) with a needle (0.25G/0.3G) attached at temperature of 37 °C and platform temperature of 10 °C with printing speed of 6 mm/s, extrusion speed of 7 mm/s. The printed 3D model was designed using a CAD/CAM software (Solid Works). The infill geometry of model is grid, and the infill density is 22%. The model is at size of 10 × 10 mm or 15 × 15 mm with line spacing of 1.2 mm, layer height of 0.2 mm and scaffold height of 0.8 mm. After the SA/PVA/HACC hydrogels were crosslinked by immersion in 4% $CaCl_2$ (w/v) solution for 2 h, the scaffolds were frozen at −20 °C for 12 h and thawed at −4 °C for 12 h, and repeated the process of freeze–thaw by three times.

2.2.3. Preparation of double-layer asymmetric scaffold

The SA/PVA/HACC ink with 500 μL was used to coat on between electrostatically spun membrane of PCL/PLA and 3D printed hydrogel of SA/PVA/HACC uniformly. Then the obtained double-layer asymmetric scaffold of PP/SPH were incubated at 37 °C for 2 h until the solution formed a hydrogel to bond the two layers.

2.3. Physicochemical properties of the asymmetric scaffold

2.3.1. Scanning electron microscopy

The surface structure of electrostatically spun films and 3D printed hydrogels were observed by field emission scanning electron microscopy (SEM) (JEOL JSM-7100F, Japan). Prior to testing, samples were dried in a vacuum freeze dryer at −90 °C for 24 h to remove moisture, and each sample was sputtered with platinum (Pt).

2.3.2. Printability evaluation

When the printing ink is in an ideal gelation state, the extruded filament will exhibit a clear morphology with smooth surface and constant width in the three-dimensional space, forming a regular grid of square pore structure. In addition, when the printing ink is in the under-gel state, the extruded filament will exhibit a droplet state and the lines between the upper and lower layers appear to fuse [38]. The Pr value is calculated using the following formula. Herein, L represents perimeter and A represents area. For the ideal printability, the interconnected channels of the constructs are square with a Pr value equal to 1.0 [39]. To calculate the Pr value, images of the printed constructs were analyzed by Image-J software to determine the perimeter and area of the interconnection channel (n = 5).

$$\mathrm{Pr} = \frac{L^2}{16A} \tag{1}$$

2.3.3. Fourier infrared spectroscopy

Fourier transform infrared (FTIR) spectra of the scaffolds was recorded using a FTIR spectrometer (Bruker Alpha, Germany). FTIR spectra of different samples were prepared by using potassium bromide (KBr, Aladdin, USA) pellet method.

2.3.4. Determination of wettability and porosity

The water contact angle (WCA) of the nanofiber membrane was measured by a water contact angle meter (AST VCA Optima S, China) in range of 0 ~ 180°, resolution of 0.01° and speed mode of 30 ~ 300 frames/sec to determine the hydrophobicity of the material, and the PCL/PLA sample was cut into smaller pieces for testing.

The porosity of the material was measured via using the liquid displacement method. PCL/PLA and SA/PVA/HACC samples were freeze-dried prior to testing. The specific gravity bottle filled with ethanol is weighed as Z_1; the mass of the sample is weighed as Z_2 and then was put into the bottle, soon ethanol was added to fill the bottle and weighed, and the mass is Z_3; the sample (sample pores filled with ethanol) is removed from the bottle, the bottle remaining ethanol was weighed as Z_4. The porosity K% of the material is as follows:

$$\mathrm{K}\,(\%) = \frac{Z_3 - Z_4 - Z_2}{Z_1 - Z_4} \times 100 \tag{2}$$

2.3.5. Swelling rate and water content

The swelling behavior and water absorption capacity of the hydrogels in physiological saline were determined by gravimetric method. Preprinted grid hydrogels (n = 5, d = 10 mm, h = 0.8 mm) were pre-frozen in a refrigerator at −20 °C and then freeze-dried in a freeze-dryer (Bilon FD-1A-80, Shanghai, China) to obtain lyophilized hydrogels with the weight recorded as W_0. The hydrogels were immersed in saline at 37 °C for a certain time, and then the surface liquid was removed and the weight W of the swollen hydrogel was measured to calculate the swelling ratio of the hydrogel [40]. The swelling ratio of the hydrogel was calculated by equation (3) as follows.

$$\text{Swelling ratio}\,(\%) = \frac{\mathrm{W} - \mathrm{W}_0}{\mathrm{W}_0} \times 100 \tag{3}$$

The water content of the hydrogel (n = 5) was calculated by equation (4). After removing the surface liquid with filter paper and weighing the swollen hydrogel (W), the hydrogel was dried in a vacuum freeze dryer at −90 °C for 24 h and weighed as W_0.

$$\text{Water content}\,(\%) = \frac{\mathrm{W} - \mathrm{W}_0}{\mathrm{W}} \times 100 \tag{4}$$

2.3.6. Mechanical test

The tensile mechanical properties of dumbbell-shaped specimens of hydrogel and electrostatic spinning film were determined using a universal testing machine (Instron 5544, US) and a 50 N load cells at a loading rate of 20 mm·min^{-1} according to ASTM D882 Standard. The compressive mechanical properties of the hydrogels were determined at a loading rate of 0.3 mm·min^{-1} using 5000 N pressure elements according to ASTM D3410-75 Standard. The stress (σ_t) was measured by the following equation (5):

$$\sigma_t = \frac{F}{S} \tag{5}$$

where σ_t is the nominal stress and S is the cross-sectional area of the material. The strain (ε_t) is defined by equation (6):

$$\varepsilon_t\,(\%) = \frac{\Delta L}{L_0} \times 100 \tag{6}$$

where, ΔL is the amount of change in length relative to the standard length of the independent specimen and L_0 is the standard length of the independent specimen [41]. Tensile strength and elongation at break are the tensile stress and strain at break respectively, and compressive strength is 60% of the strain strength. Tensile and com-

pressive moduli of elasticity were calculated in the strain range of 5 ~ 10%, which the relationship of stress–strain is linear. Three duplicate samples were tested in triplicate.

2.4. Proliferation of cells on scaffolds

2.4.1. Culture of human dermal fibroblasts (HFBS)

All samples were lyophilized and sterilized under UV light. Samples were then washed three times with Dulbecco 's Modified Eagle medium (DMEM, Gibico, USA) before use. HFBS cells (Shanghai Cell Bank, Chinese Academy of Sciences) were incubated in DMEM supplemented with 10% fetal bovine serum (FBS, Gibico, USA) and 1% antibiotics (Gibico, USA) at 37 °C with 5% CO_2 (Thermo Forma 311 direct heat CO_2 incubator, USA). HFBS cells were digested with 0.05 % trypsin and then suspended in fresh medium. The pretreated hydrogel samples were placed on the bottom of 24-well cell culture plates, on which 1×10^4 cells were inoculated. In addition, spun film samples were inoculated with 5×10^3 cells on the bottom of 48-well cell culture plates to observe the cell adhesion on each sample. The spun bond samples were circular plates with a diameter of 6 mm and a thickness of 0.5 mm, and the grid hydrogel samples had a side length of 10 × 10 mm and a thickness of 0.8 mm. The morphological changes of cells were observed by fluorescent inverted microscope (Nikon, TiS, Japan) at 1, 3 and 5 days, respectively.

2.4.2. CCK-8 proliferation assay

Cell Counting Kit-8 (CCK-8) was used to detect the proliferation of HFBS cells on 1, 3 and 5 days (n = 3). Each sample was inoculated with cells in well plates, containing 1 mL of DMEM with 10% fetal bovine serum and 1% antibiotics in per well. At each time point, the culture medium was replaced with DMEM medium containing 10% CCK-8 solution and incubated for 2 h. At the end of the incubation, 300 μL of culture medium was removed from each well into a new 96-well plate. The absorbance at each time point was measured with an enzyme marker at 450 nm (Bio-Rad iMark, USA).

2.4.3. Live-Dead staining

Samples were washed three times in DMEM before use. The cell viability of the samples was measured using the LIVE/DEAD viability/cytotoxicity kit. LIVE/DEAD staining was performed using calcitanin-AM and ethidium-1, with which live cells were stained green and dead cells were stained red. A concentration of 1×10^4 cells/mL was inoculated on hydrogel scaffold samples in 24-well plates, and spun membrane samples were inoculated with 5×10^3 cells on the bottom of 48-well cell culture plates for 1, 3, and 5 days. After the medium in the well plates was removed, each sample was rinsed with DMEM, and then 200 μL of calcitanin-AM and ethidium-1 (1:2, v/v) with DMEM was injected into the well plates. The well plates were immediately placed in the dark at 37 °C with 5% CO_2 for 30 min. After that, all samples were rinsed three times with DMEM and observed with a fluorescent inverted microscope, and spun membrane samples were operated similarly.

2.5. Antimicrobial properties of the asymmetric scaffold

The antimicrobial activity of the SA/PVA/HACC printed hydrogel inner layer was determined using the inhibition loop method [42]. Firstly, *Staphylococcus aureus (S. aureus)* and *Escherichia coli (E. coli)* were used as Gram-positive and Gram-negative bacteria models, and purified and diluted to 10^6 cfu/mL. The 100 μL of bacterial solution was coated evenly after solidification of the solid medium, and round plate samples with a diameter of 6 mm were taken and placed in Petri dishes, respectively, and then incubated in a constant temperature incubator at 37 °C for 24 h. After the inhibition ring appeared around the samples, the diameter of the inhibition ring was measured by vernier calipers and recorded. Three parallel tests were performed for each group of samples.

2.5.1. Analysis of bacterial penetration into the outer layer of the PCL/PLA membrane

In addition, the ability of the PCL/PLA composite nanofiber membrane to provide a barrier to external microorganisms on the trauma surface was also evaluated by with bacterial models (*S. aureus* and *E. coli*), and then the bacteria on surface of the upper and bottom of the fiber membranes were observed by SEM. *S. aureus* and *E. coli* were used to evaluate the ability of hindering bacterial penetration from upper layer of the membrane to bottom layer respectively. The 1×10^6 cfu/mL of bacterial suspension was inoculated on PCL/PLA (n = 3) membranes at 37 °C for 24 h. In addition, the presence of microorganisms on the upper and bottom surfaces of samples was observed by SEM.

2.5.2. The antibacterial activity of 3D printed hydrogels

The antibacterial properties of the 3D printed SA/PVA/HACC hydrogels were characterized using a modified Kirby-Bauer technique [43]. For this purpose, round hydrogels (n = 3) with vancomycin (VCM) and HACC were placed on the surface of agar plates containing *S. aureus* or *E. coli* (1×10^6 cfu/mL) and incubated for 24 h at 37 °C. Then, the image analysis software of Image J (Scion Corp., Frederick, MD) was used to photograph the inhibition ring around the samples and to determine the diameter of the ring.

2.6. Statistical analysis

All experiments were repeated three times. The data results were expressed as the mean ± standard deviation. One-way ANOVA was used to determine the significant difference by using SPSS, version 23 (IBM), and values were considered statistically significant at $p < 0.05$.

3. Results and discussion

3.1. The morphology and structure of optimized asymmetric dressing

The structure and morphology of asymmetric dressing was shown in the SEM of Fig. 1 and Fig. 2. Fig. 1(a) shows a 3D printed 4-layer model with a height of 0.2 mm. The inner 3D printed layer of SA/PVA/HACC appears macro-pore structure with a mean diameter of 842.76 ± 103.65 μm in Fig. 1(b), which would facilitate the exchange of nutrients to the regenerating tissue. Fig. 1(c) ~ (f) shows the macroscopic morphology of 3D 4-layer printed SA/PVA/HACC scaffolds tuning by different PVA concentrations. It can be seen that the printed scaffolds have more obvious line spacing and less line fusion to reach the moderate gel state with the increase of PVA concentration. Accordingly, the printability was introduced to optimize the printed inks. Fig. S1 (see supplementary) shows the Pr value of 2-layer printed constructs with concentration of PVA changing from 0% to 6%. The results show that the Pr value reaches 0.92 ± 0.01 as the PVA concentration is 6% (w/v), which exhibits the best shape fidelity. However, the ink cannot be extruded normally, even easy to block the needle as the concentration of PVA continues to increase from 6%. Therefore, the optimized scaffold obtained was prepared by choosing the PVA concentration of 6% (w/v), and four-layer of 3D printed hydrogel was controlled to simulate the skin dermis thickness of 0.6–3 mm [44] as the inner scaffold with SA/PVA/HACC (5:6:1, w/w/w).

Fig. 2(a) ~ (c) shows the outer layer of membrane with different PCL/PLA ratios, all of which exhibited a densely connected mesh structure. For the concentration of 18 wt% PCL, some beads appeared in Fig. 2(a). Smooth and bead-free fibers with larger

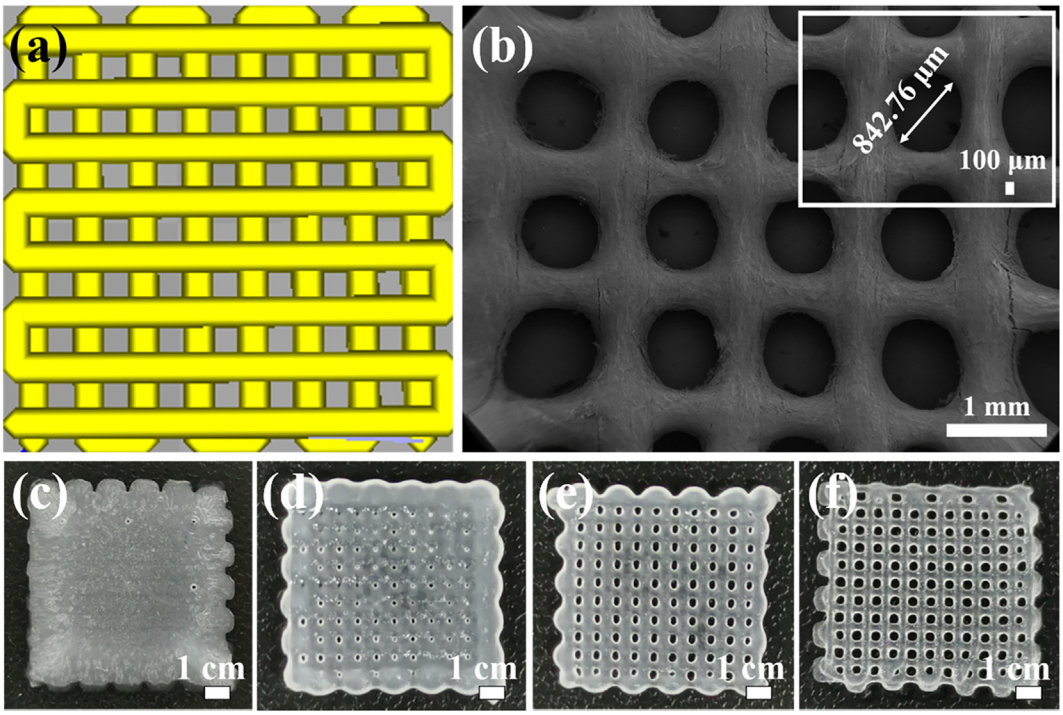

Fig. 1. (a) Schematic diagram of the software modeled print; (b) SEM morphology of the 3D printed SA/PVA/HACC substrate; the macro morphology of the underlying support with different PVA concentrations (c) 0 wt% (d) 2 wt% (e) 4 wt% (f) 6 wt% by 3D printing.

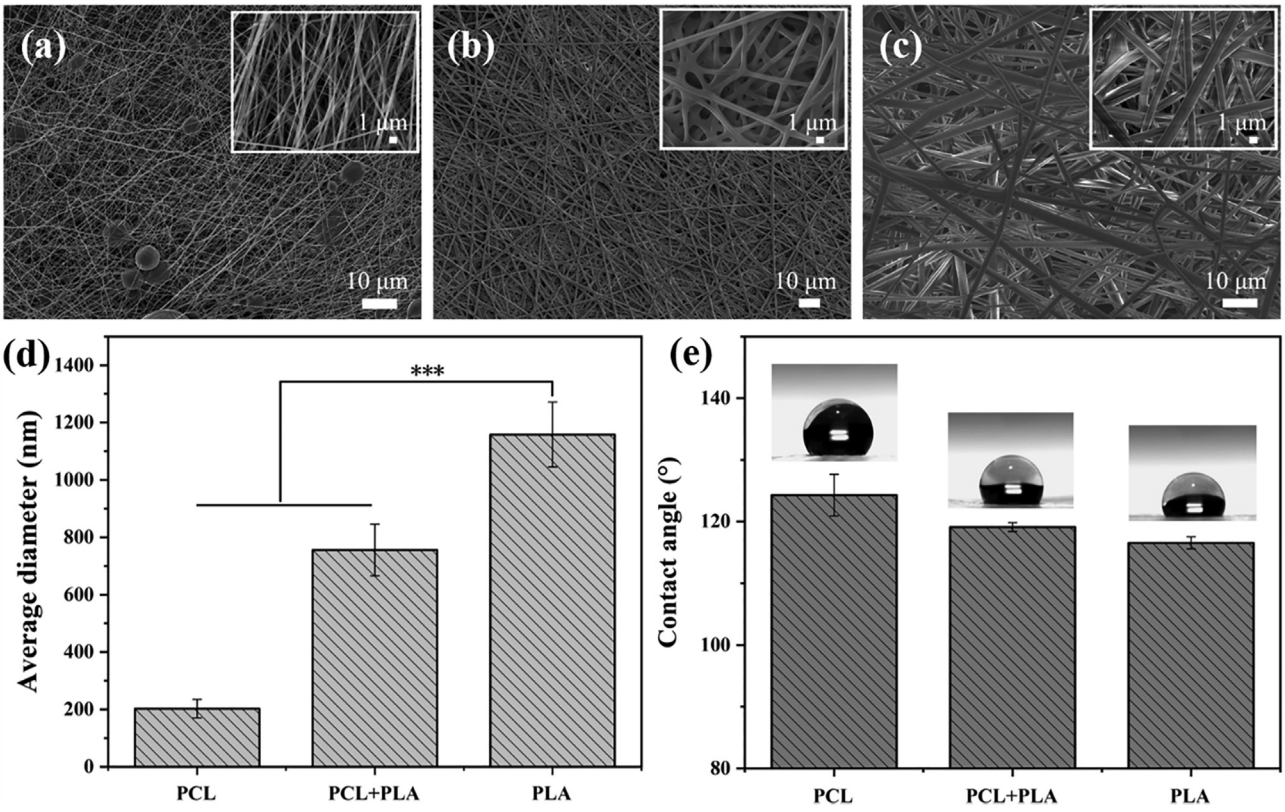

Fig. 2. SEM morphology of electrostatic spun PCL/PLA nanofiber membranes with different materials (a) 18 wt% PCL; (b) 12 wt% PCL/6 wt% PLA; (c) 18 wt% PLA; (d) average fiber diameter of different membranes; (e) water contact angle of electrostatically spun nanofiber membranes.

diameter were obtained with a higher PLA concentration (no<6 wt %) in Fig. 2(b) and (c). Fig. 2(d) shows that the average diameter of PCL/PLA composite membrane fibers was 755.9 ± 107.1 nm, comparing to pure PCL membrane of 202.6 ± 32.4 nm and pure PLA membrane of 1158.3 ± 207.5 nm. The average diameter of PCL/PLA composite membrane fibers increases with the increase of

PLA ratio, indicating that the concentration of PLA regulating the diameter of nanofibers. According to previous studies, the increase in solution viscosity is due to the increase of solution concentration, which is responsible for the increase in the average diameter of the fibers [45]. For an ideal wound healing material, bead-free fibers with smaller diameter are preferred [46], therefore 12 wt% PCL/6 wt% PLA (PCL/PLA (2:1, w/w)) was selected for electrospinning in this study. The hydrophilic polymer chains of the 3D printed hydrogel layer can effectively absorb high concentrations of aqueous exudates and maintain a moist environment at the wound site while absorbing excess exudates [47]. The nanofibrous layer also acts as a barrier to microbial infiltration with novel structure that allow exudate drainage and gas exchange, which are crucial to prevent skin infections and the occurrence of wound dehydration [48].

As shown in Fig. 3, the nanofiber membrane can be well fixed on the hydrogel inner layer, and the two parts are bonded tightly. It can be seen in SEM that the cross sections of the bilayer dressing are still visible after 1, 3, and 5 days of incubation, and remain intact shape.

The materials were characterized by FTIR spectra in the range of 4000 ~ 500 cm^{-1} with a resolution of 4 cm^{-1} as shown in Fig. S2 (see Supplementary). It can be seen that no new bonds are appeared or obviously shifted, indicating that there is no strong interaction occurred between PCL and PLA, and only physical combination in Fig. S2(a) [49]. The result suggested that PCL/PLA could

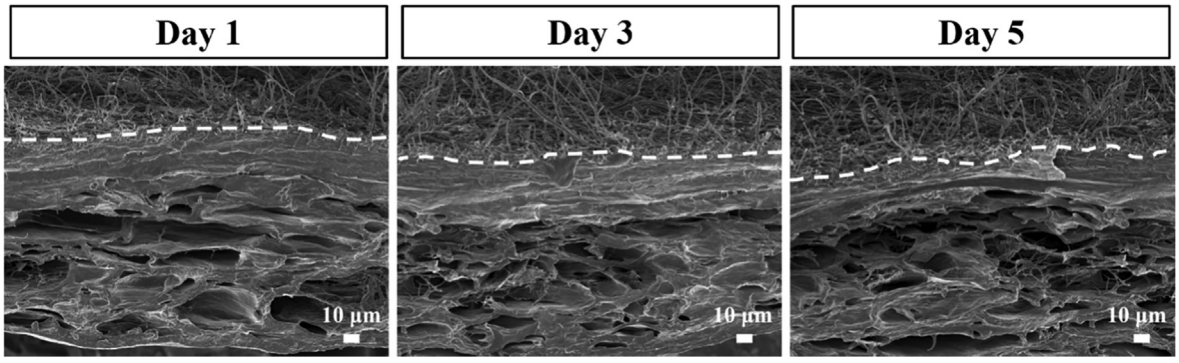

Fig. 3. SEM images of composite scaffold cross-sections after incubation in NaCl saline (pH = 7) for 1, 3 and 5 days.

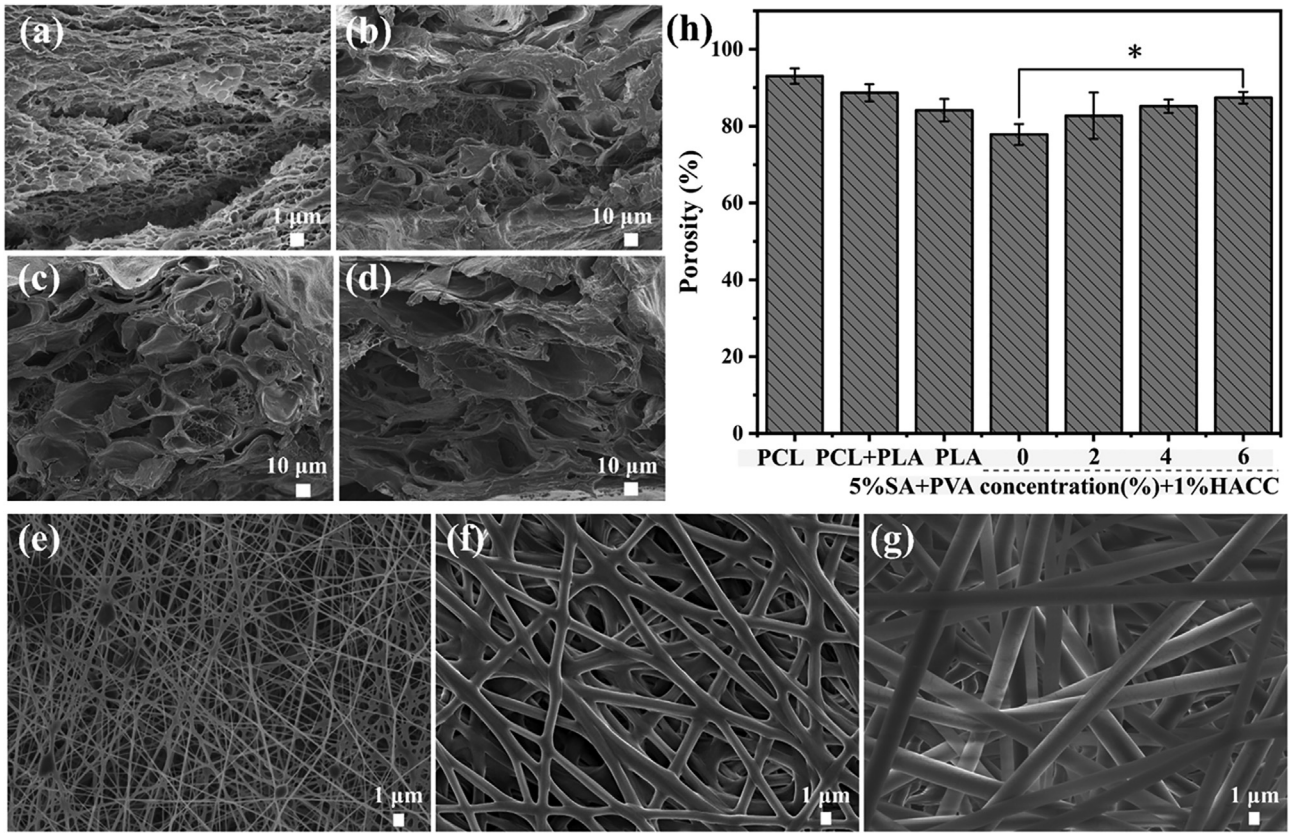

Fig. 4. SEM morphology of 3D printed SA/PVA/HACC substrate scaffolds with different PVA concentrations (a) 0 wt% (b) 2 wt% (c) 4 wt% (d) 6 wt%; SEM morphology of electrostatically spun PCL/PLA nanofiber membrane with different materials (e) 18 wt% PCL (f) 12 wt% PCL/6 wt% PLA (g) 18 wt% PLA; (h) porosity of different materials.

perform their properties of hydrophobicity of PCL and mechanical strength of PLA after electrostatic spinning, which may contribute to up to epidermis-like properties such as water-proof ability and mechanical resistance [25]. For inner 3D printed layer of SA/PVA/HACC, Fig. S2(b) shows that the SA/PVA/HACC hydrogel was marked at 1742.8 cm^{-1} (absorption band shifted from 1730.8 cm^{-1} referred to the C = O groups in PVA) indicates that the PVA are cross-linked by Freeze-thaw [50,51]. Compared with SA, PVA, and HACC groups, the SA/PVA/HACC group shows a broadening of the absorption peaks near 3300 cm^{-1} and a red-shifted trend, indicating that SA, PVA, and HACC interact with each other and form hydrogen bonds.

3.2. The wettability and porosity of scaffolds

The surface wettability represents the ability of the liquid to spread on the solid phase surface [52]. The wettability of wound dressings can be evaluated by measuring the WCA [53,54] (Fig. 2e). The WCA value of PCL/PLA film was 119.1 ± 0.72°, showing a hydrophobic contact angle (90° < WCA < 180°). The hydrophobicity of the solid surface is closely related to its surface energy, with a low solid surface energy and a large static water contact angle, showing significant hydrophobicity when the WCA is greater than 90° [55]. This result can be caused by the high percentage of hydrophobic groups, such as hydrocarbon and ester groups on the chains of PCL and PLA polyesters, which allow wounds to avoid the risk of wet water.

Fig. 4(a)∼(d) shows the SEM images of the cross section structure of SA/PVA/HACC hydrogels with different PVA ratios. As seen from the figures, the hydrogels show a uniform three-dimensional porous structure, and the pore size becomes larger with the increase of PVA content. It can be seen that the internal pores of SA/PVA/HACC hydrogels are interconnected with each other, which can be speculated as the interaction of hydrogen bonding and crystalline regions to produce physical crosslinking, thus forming a three-dimensional porous structure. Fig. 4(e)∼(g) shows the SEM images of different component ratios of PCL/PLA composite membranes. It can be seen that the surface structure of the composite membranes possess interconnected porous structure at all three ratios, which would be conducive to gas exchange for wound healing [56].

The porosity of both the electrostatic spun outer layer and the 3D printed inner layer is between 70 ∼ 90% as shown in Fig. 4 (h), which is consistent with the porosity values reported in the literature [57]. These connected pores facilitates the exchange with external gases as well as the transport of nutrients and metabolic waste [58].

3.3. The swelling rate and moisture content of the scaffolds

The healing process is associated with the production of wound exudate, and excess exudate can prevent cell migration to the wound surface, thereby prolonging the wound healing period [59]. In this study, the swelling rate and water absorption rate of

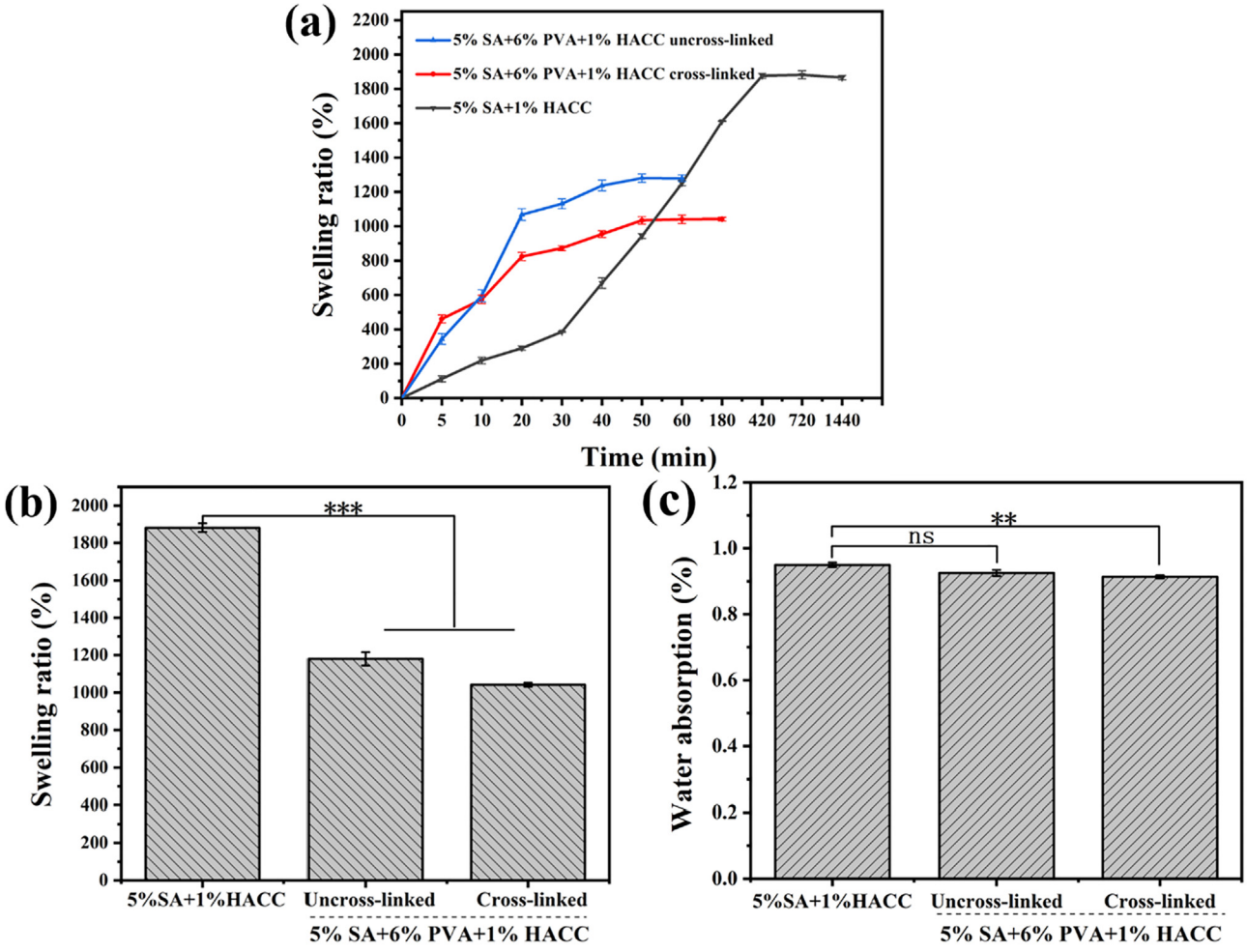

Fig. 5. Evaluation of the properties of 3D printed SA/PVA/HACC substrate scaffolds. (a) swelling process (%); (b) swelling ratio (%); (c) water absorption (%).

hydrogel inner layer was tested in equilibrium state at each time point, which represents its ability to absorb trauma exudate. In order to simulate the neutral physiological environment of human body, 0.9% NaCl (w/v) solution with neutral was chosen as the swelling environment in this experiment to study the swelling and water content characteristics of SA/PVA/HACC hydrogel in 37 °C (Fig. 5).

The SA/PVA/HACC (cross-linked) hydrogels reached equilibrium swelling (1041.4 ± 11.2) % for about 60 min (Fig. 5a), and the swelling rate of the hydrogels with PVA was reduced compared to the SA/HACC hydrogels due to the increase of hydrophilicity. But freeze–thaw crosslinking of PVA may increase binding sites and crosslinking degree, resulting in a more compact and strong structural bonding within the hydrogel, which leads to lower swelling. It can be seen that the equilibrium swelling rate of SA/PVA/HACC (cross-linked) is the lowest (Fig. 5b), which may be due to the increase in the matrix density of the hydrogel with cross-linking of PVA [60]. Therefore, the lower swelling rate and good water absorption properties facilitate the absorption of wound exudate and maintain the environmental humidity while promoting the healing process. In addition, all hydrogels were in swelling equilibrium, there was no significant difference in the water absorption rate of hydrogels (Fig. 5c), and the water content was above 85%. Therefore, the SA/PVA/HACC hydrogels prepared in this study have good swelling properties and water absorption ability.

3.4. The mechanical properties of scaffolds

To investigate the mechanical properties of the samples, electrospun PCL/PLA nanofiber films and SA/PVA/HACC hydrogel scaffolds were performed tensile test in a humid environment, respectively, and the results are shown in Fig. 6 and Fig. 7. Fig. 6 shows that the tensile modulus and tensile strength of the composite PCL/PLA nanofiber membranes was (19.69 ± 0.66) MPa and (1.24 ± 0.03) MPa, respectively, and the elongation at break could reach (50.21 ± 3.03) %. PCL and PLA blends have better results than PCL or PLA alone in improving the mechanical properties of the scaffolds by adjusting the ratio of PLA and PCL in the composite [25]. Therefore, the optimized PCL/PLA composite film with moderate average fiber diameter and good mechanical strength was selected as the outer layer of the dressing in this study. While the elongation at break of 3D printed SA/PVA/HACC scaffold increased with the increase of PVA content, the elongation at break of SA/PVA/HACC composite scaffold with 6% PVA (w/v) could reach (74.54 ± 1.71) %, which was significantly higher compared to SA/HACC scaffold (56.01 ± 2.74) % in Fig. 7. This could be attributed to the increased concentration of PVA and degree of cross-linking within the hydrogel, resulting in the subsequent enhancement of mechanical properties. These results confirm that the dressings made in this study have good mechanical properties, which conform to the mechanical range for natural skin of tensile strength

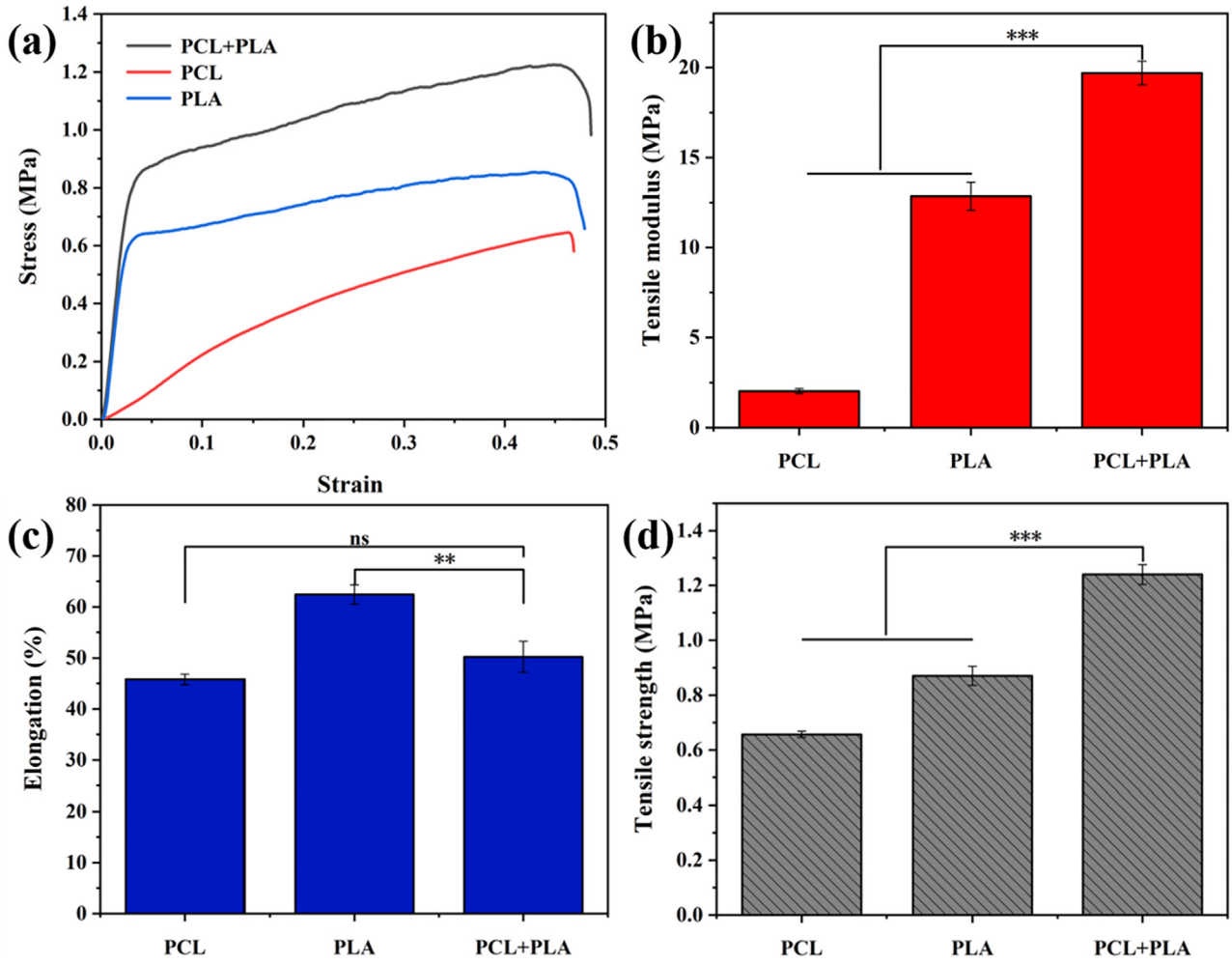

Fig. 6. Tensile properties of electrostatically spun PCL/PLA nanofiber films (a) stress–strain (MPa); (b) tensile modulus (MPa); (c) elongation at break (%); (d) tensile strength (MPa).

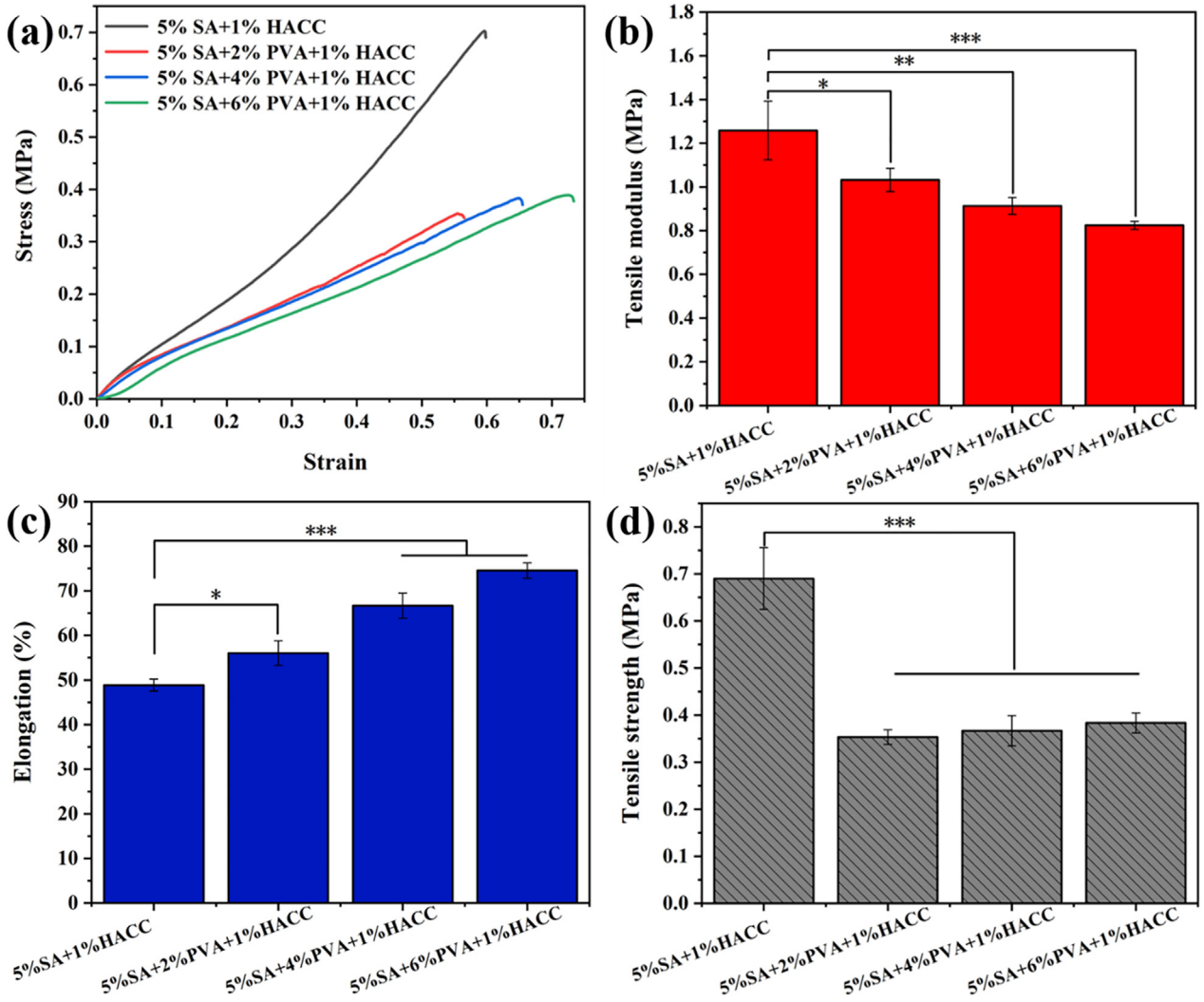

Fig. 7. Tensile properties of 3D printed SA/PVA/HACC hydrogel substrates (a) stress–strain (MPa); (b) tensile modulus (MPa); (c) elongation at break (%); (d) tensile strength (MPa).

(5 ~ 30 MPa), Young's modulus (4.6 ~ 20 MPa) and elongation at break (35 ~ 115 %) [61,62,63].

In addition, the compressive property was characterized in Fig. 8. It can be seen that the compressive modulus and strength of the scaffold were (0.53 ± 0.01) MPa and (0.75 ± 0.02) MPa with 6% PVA (w/v) respectively, which significantly higher than those of the SA/HACC scaffold (0.4 ± 0.01) MPa, (0.45 ± 0.01) MPa, respectively ($p < 0.001$), and increasing significantly with the increase of PVA content. This may be due to the improvement of mechanical strength of the hydrogels through cyclic freeze thawing, which caused by the formation of physical crosslinks between PVA and SA in the composite hydrogels by inter- or intra-molecular hydrogen bonding and crystallization regions [64,65]. In addition, the compressive strength values of SA/PVA/HACC composite hydrogels were close to those of natural skin (0.2–7 MPa) [66], indicating that the SA/PVA/HACC composite scaffold prepared in this study possess mechanical compatibility for the inner layer of wound dressings.

There are some commercial wound dressings, and 3 M™ Tegaderm™ Alginate Ag Silver Dressing is a highly absorbent nonwoven antimicrobial dressing, composed of high guluronic acid calcium alginate, carboxymethylcellulose, and an ionic silver complex (silver sodium hydrogen zirconium phosphate) developed by 3 M Medical (USA). It has a tensile strength of 0.14 MPa and an elongation of 27.4% [67 68]. Whereas, the tensile strength of the composite PCL/PLA nanofiber membranes was (1.24 ± 0.03) MPa, and the elongation at break could reach (50.21 ± 3.03) % in this study. The tensile strength and the elongation of SA/PVA/HACC composite scaffold with 6% PVA (w/v) could reach (0.38 ± 0.02) MPa and (74.54 ± 1.71) %, respectively. Therefore, the PP/SPH have higher tensile strength and elongation than the 3 M™ Tegaderm™ Alginate Ag Silver Dressing in this study.

3.5. In vitro cell culture studies

3.5.1. Cytotoxicity screening for bilayered scaffolds

Biocompatibility is an important characteristic in the study on biomedical materials for tissue or organ repair [45]. The asymmetric bilayer scaffolds prepared in this experiment were co-cultured with HFBS for 1, 3, and 5 days and used to assess their cytotoxicity. In Fig. 9(a), the proliferation of HFBS on nanofibrous membranes was assessed using the CCK-8 test. The experimental group was PCL/PLA composite membrane with different proportions, while the blank control group was without material group. The differences between the experimental and blank control groups at each time point (1, 3 and 5 days) were statistically significant, and the absorbance values of the experimental groups increased significantly with the increase of the incubation time. At the same time

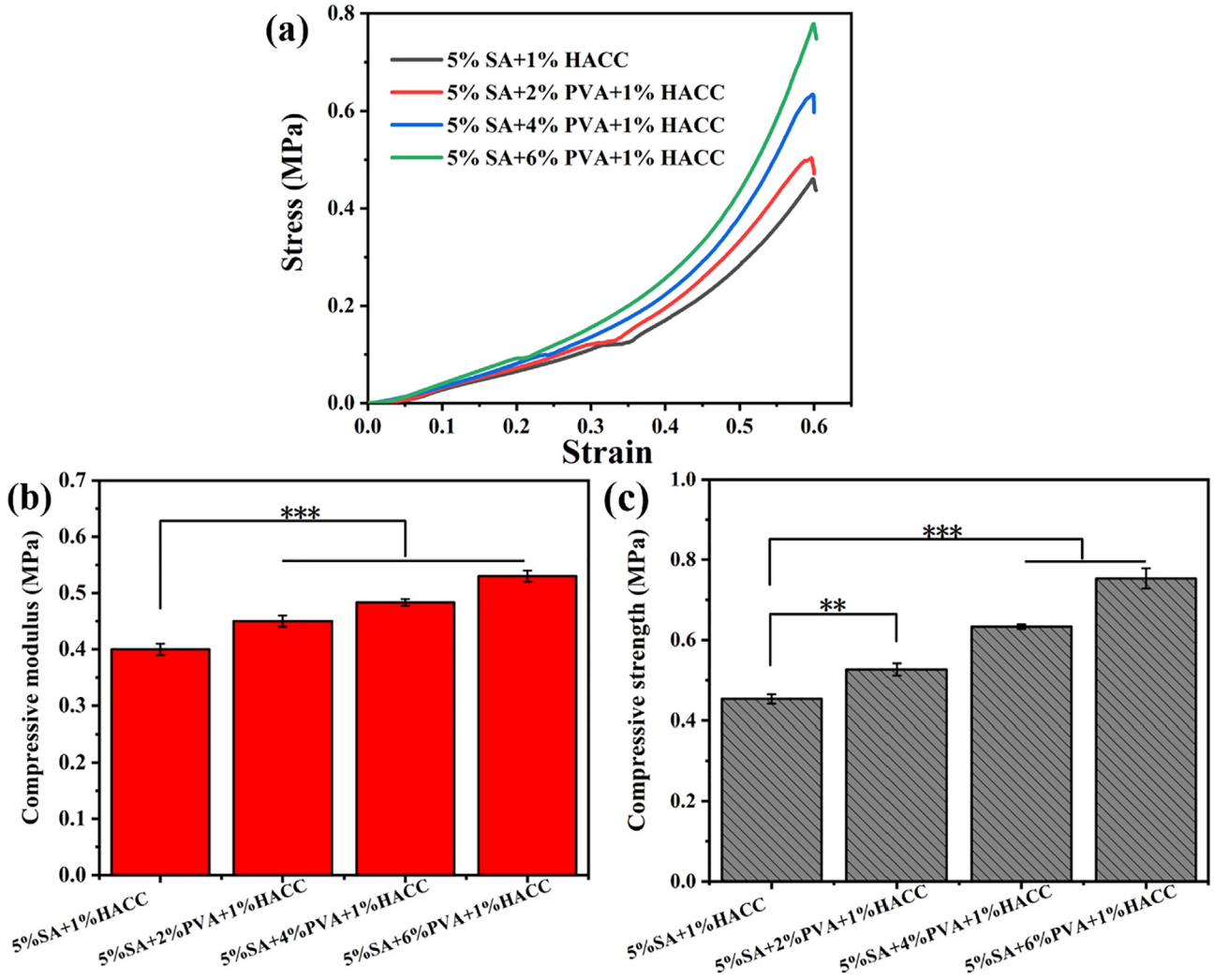

Fig. 8. Compression properties of 3D printed SA/PVA/HACC hydrogel substrates (a) stress–strain (MPa); (b) compression modulus (MPa); (c) compressive strength (MPa).

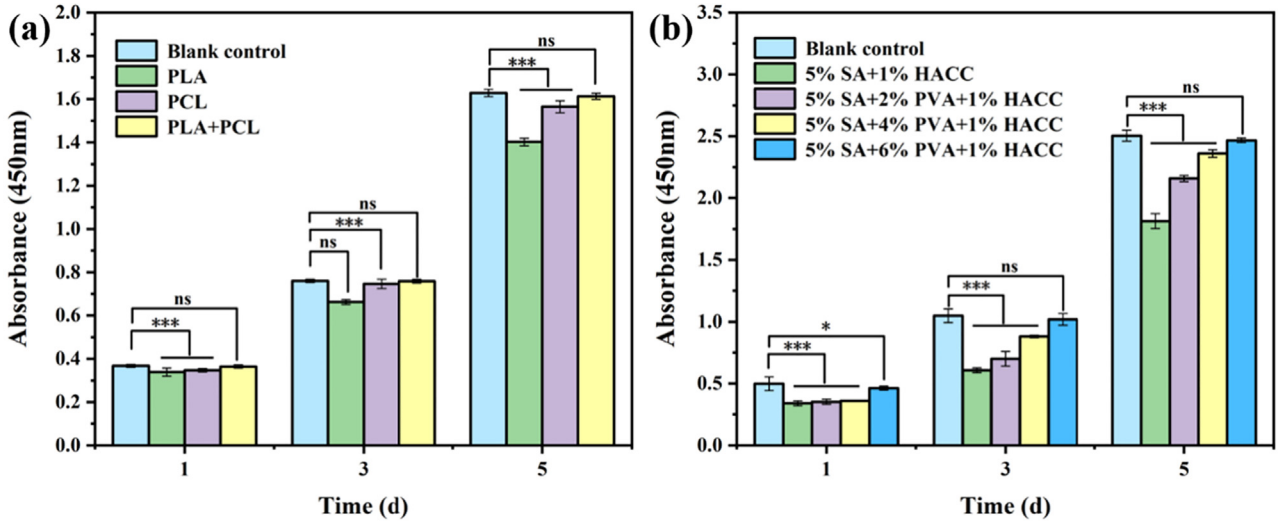

Fig. 9. CCK-8 test to detect proliferation of HFBS cells co-cultured with PP/SPH bilayer scaffolds (a) electrostatic spun PCL/PLA nanofiber membrane; (b) 3D printed SA/PVA/HACC hydrogel substrate, error bars indicate standard deviation of the mean, *p < 0.05,**p < 0.01,***p < 0.001 (n = 3).

point, there was no significant difference in absorbance values between the PCL/PLA group and the blank control group. In the PLA membrane group, the low wettability and lack of specific functional groups for cell growth on the surface of PLA may cause poor cell proliferation, resulting in lower absorbance value compared with other experimental groups [69]. Fig. 9(b) shows the proliferation of HFBS cultured on 3D printed hydrogel layer for 1, 3 and 5 days. Herein, the experimental groups were SA/PVA/HACC hydrogels with PVA concentrations of 0, 2, 4, 6% (w/v), and the blank control group was without material group. The absorbance values of the experimental groups increased significantly with the increase of incubation time. However, the absorbance values of SA/HACC group were lower compared with other groups containing PVA, may due to the easier decomposition of SA/HACC comparing to other group and then producing gel fragment in this study. Large molecular debris may occupy the living space of cells, hindering the cell culture space and limiting cell proliferation [70,71]. With the increase of PVA concentration, the hydrogel structure is stronger and the gel fragments are reduced or even disappeared, which provides a friendly environment for cell growth and proliferation is obvious. At the same time point, there was no significant difference between the absorbance values of SA/PVA/HACC group with 6% PVA (w/v) and blank control group. Therefore, when HFBS were co-cultured with the asymmetric bilayer scaffold prepared in this

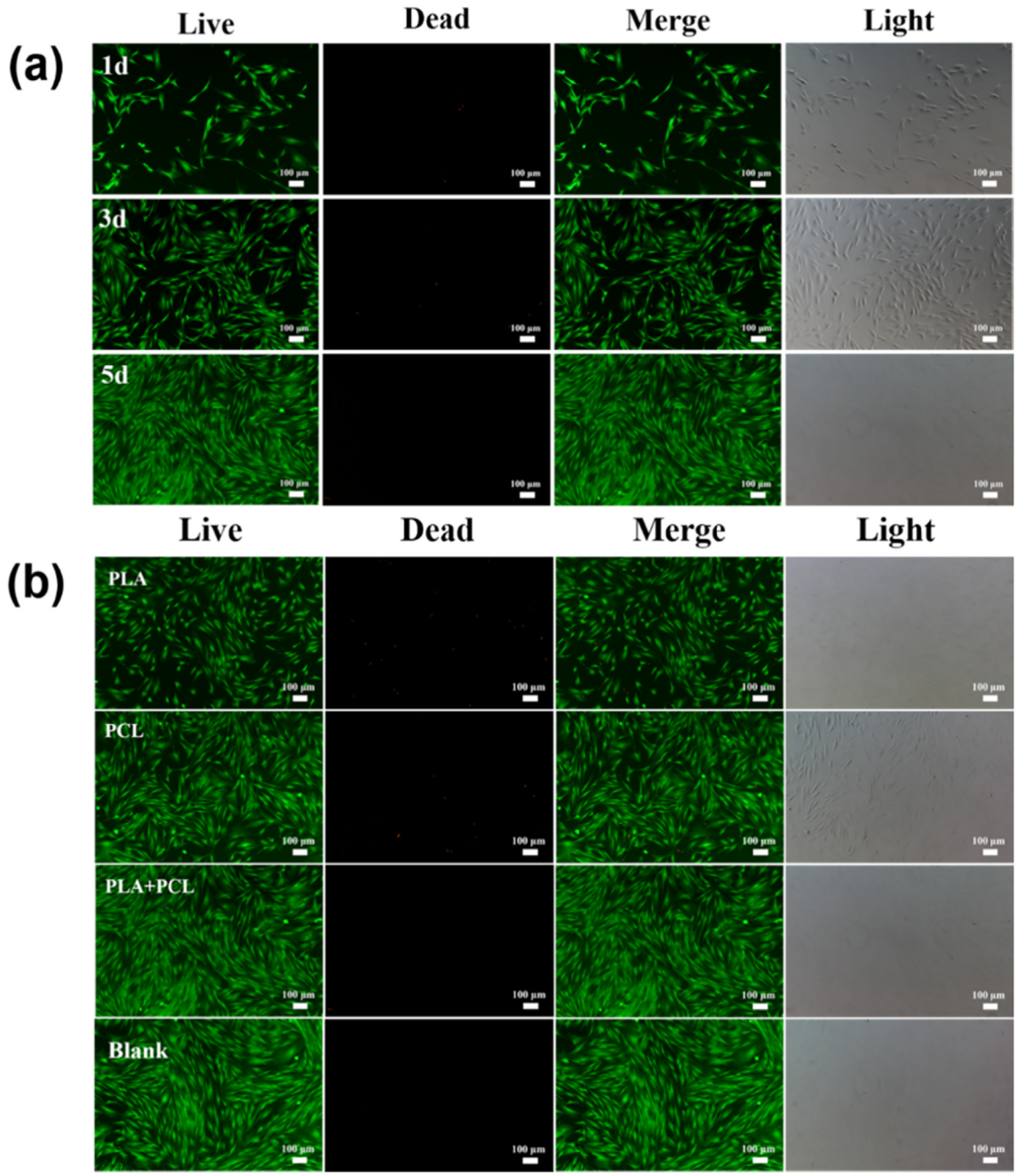

Fig. 10. Live/dead staining images of HFBS after co-culture with PP/SPH bilayer scaffolds. (a) HFBS co-cultured with PCL/PLA nanofiber membranes after 1, 3, and 5 days; (b) HFBS co-cultured with different ratios of nanofibrous membranes for 5 days; (c) HFBS co-cultured with SA/PVA/HACC hydrogel substrates with 6% PVA (w/v) content for 1, 3, and 5 days; (d) HFBS co-cultured with hydrogel substrates of different PVA ratios for 5 days.

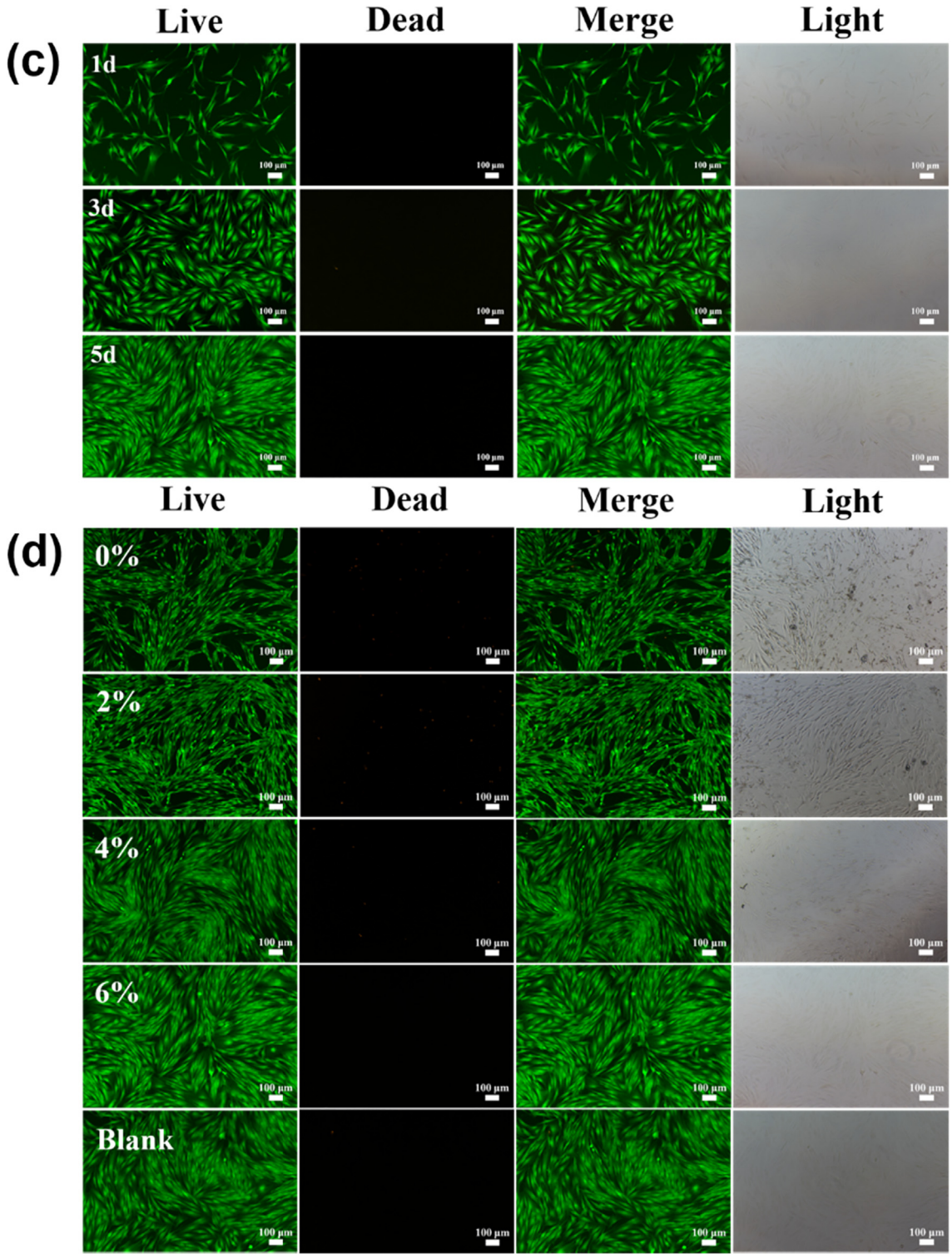

Fig. 10 (*continued*)

experiment, the cells all showed significant proliferation with the extension of the culture time, indicating that the material has good cytocompatibility and can maintain normal growth and proliferation of HFBS.

3.5.2. Cytoskeletal staining

The Live/Dead assay (LDA) is a two-step staining method in which live cells are stained green and dead cells are stained red, and is used to study the viability of cells on bilayer scaffolds for 24, 72 and 120 h. As seen in Fig. 10, HFBS proliferated and still survived well on the substrate by observing cellular morphology under fluorescence microscopy, and the density of live cells increased with the increase of culture time. At 72 h, the cell density on the bilayer scaffold was significantly greater than that at 24 h. A small number of dead cells were detected by low bright red fluorescence, which was similar to that of the control group, indicating

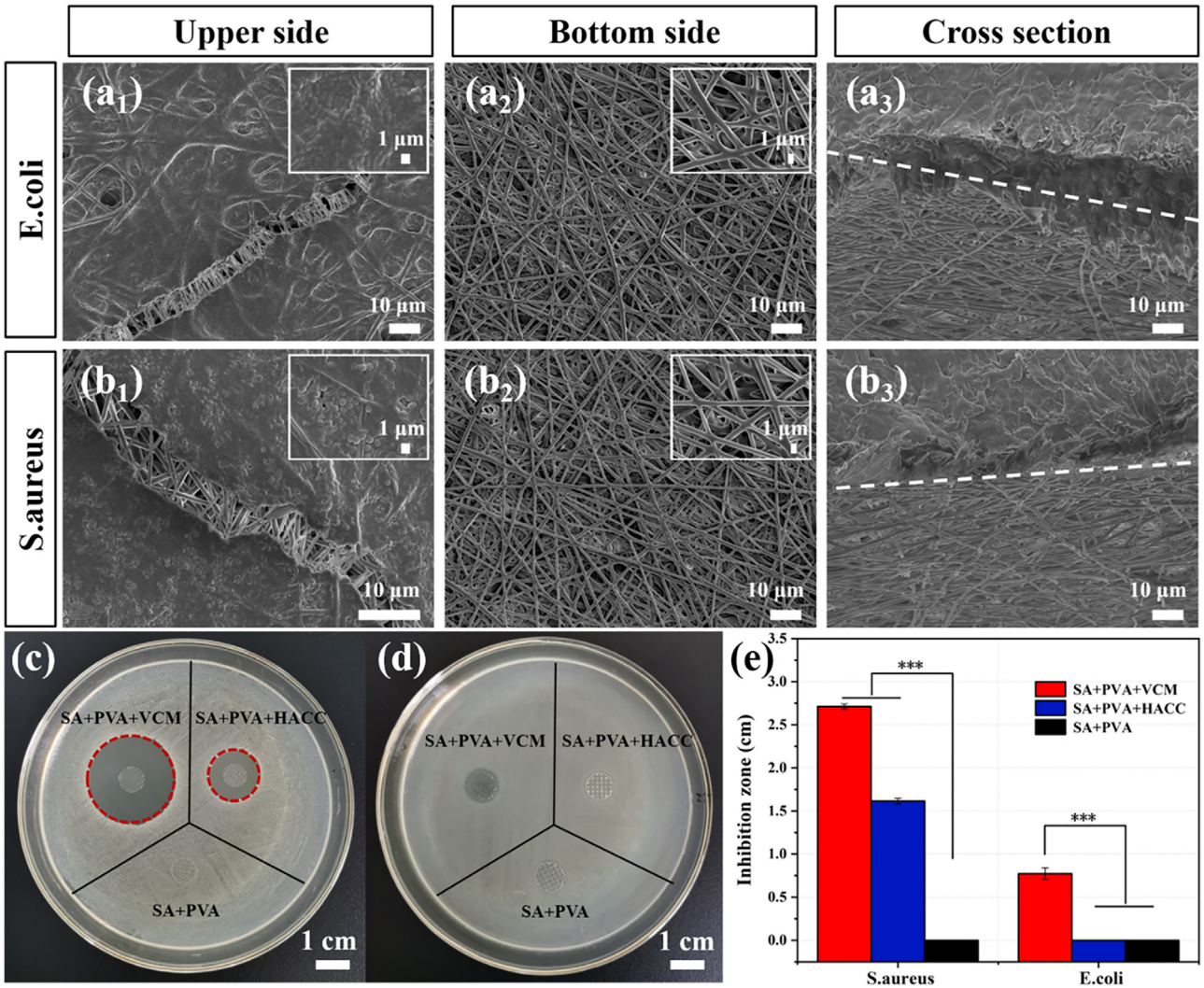

Fig. 11. Outer layer of electrostatically spun PCL/PLA nanofiber membrane blocking microorganisms (a_1) *E. coli* attached to the upper of the membrane (a_2) bottom of the membrane (a_3) cross section of the membrane; *S. aureus* attached to (b_1) upper of the membrane (b_2) bottom of the membrane (b_3) cross section of the membrane; (c) inhibition circle of *S. aureus* (d) inhibition circle of *E. coli* on the bottom layer of 3D printed hydrogel; (e) diameter analysis of the inhibition circle.

that the asymmetric bilayer scaffold prepared in this experiment without obvious cytotoxic effects on HFBS. And the asymmetric scaffold had good cytocompatibility, which was consistent with the result of CCK-8 test mentioned above.

3.6. Antibacterial activity of scaffolds

Most infections of body tissues are mainly caused by *S. aureus* and *E. coli* accompanied by implanting materials [72]. Gram-positive *S. aureus* is found in the initial stages of the infection process, and Gram-negative *E. coli* is involved in the later stages of the infection process [73]. Therefore, *S. aureus* and *E. coli* were chosen as template bacteria to evaluate the blocking ability of the fibrous membrane for bacteria in this study, and the results are shown in Fig. 11(a) (b). As seen in Fig. 11(a_1) (a_2) (b_1) (b_2), although some bacteria could attach to the upper surface of the nanofiber layer and even form a biofilm, a clear demarcation between the upper and bottom layers can be seen in the cross section in Fig. 11(a_3) (b_3), and the bacteria did not penetrate from the upper to the bottom of the PCL/PLA nanofiber layer. It shows that the porous fiber membrane on the outer surface layer acts as a protective barrier and hinders the penetration of both bacteria.

In addition, the ability of SA/PVA/HACC hydrogel to provide an antibacterial environment was also evaluated. In Fig. 11(c), both the hydrogel loading VCM and the hydrogel scaffold with HACC appeared inhibition ring of 2.71 ± 0.29 cm and 1.61 ± 0.35 cm in diameter for *S. aureus*, respectively, whereas the SA/PVA hydrogel without VCM and HACC did not show any obvious inhibition circle around the inhibition plate. SA/PVA/HACC hydrogel has certain inhibition of *S. aureus*, in which the inhibition of HACC can achieve obvious inhibition effect and avoid the use of antibiotics. The results in Fig. 11(d) showed that HACC did not show resistance to *E. coli*, and no obvious inhibition circle was seen around the material, while VCM had little inhibitory effect on *E. coli*. The data in Fig. 11(e) also showed that HACC showed some inhibition against *S. aureus*, but not against *E. coli*. This fact is due to the HACC polymer is generally more active against Gram-positive bacteria than against Gram-negative bacteria. The surface of bacteria is mostly negatively charged proteins and lipopolysaccharides, whereas HACC is a kind of cationic polymer, will interact electrostatically with bacterial surfaces to disrupt cell membranes, leading to leakage of K^+ and other cytoplasmic components from inside to outside the cell membrane, thus hindering bacterial growth and reproduction [74].

4. Conclusion

In this study, we fabricated a novel asymmetric bilayer wound dressing scaffold by optimizing composites with composition of PCL/PLA (2:1, w/w) and SA/PVA/HACC (5:6:1, w/w/w) through electrostatic spinning and 3D printing method, mimicking the inherent gradient structure and function of the epidermis and dermis of natural skin [75]. In the developed bilayer wound dressing, the outer layer of the asymmetric dressing was made by a dense and interconnected polymeric nanofibrous PCL/PLA membrane with hydrophobic properties, which act as physical protective barrier to the wound site. It was able to resist the microorganisms' infiltration and present excellent mechanical properties including tensile strength, young modulus, and elongation at break, similar to natural human skin. On the other side, the 3D printing technique was used to construct the dermis structure with larger pore size by promoting the sequential layer-by-layer deposition of the SA/PVA/HACC. This layer acts as a porous structural template with good printability, also exhibiting better mechanical properties, keeping a moist wound environment, good water absorption ability as well as inhibiting the *S. aureus* growth. Furthermore, *in vitro* cell culture results showed that the PCL/PLA and SA/PVA/HACC scaffolds were non-toxic to HFBS, favorable to cell proliferation. Overally, this study fabricates wound dressings with excellent mimicking gradient multifuctional properties, and it would be an efficient as well as safe regeneration strategy in skin repair.

CRediT authorship contribution statement

Ting Zhang: Writing – original draft, Writing – review & editing, Investigation. **Hao Xu:** Writing – review & editing, Investigation. **Yonggang Zhang:** Resources, Validation. **Siruo Zhang:** Investigation. **Xia Yang:** Resources, Supervision. **Yan Wei:** Resources, Supervision, Funding acquisition. **Di Huang:** Resources, Supervision, Funding acquisition. **Xiaojie Lian:** Project administration, Supervision, Resources, Funding acquisition, Validation.

Declaration of Competing Interest

The authors declare that they have no known competing financial interests or personal relationships that could have appeared to influence the work reported in this paper.

Acknowledgments

This work was supported by the Natural Science Foundation of Shanxi Province, China (No. 20210302123132 and 201901D111077), the Key Research and Development Program of Shanxi Province, China (International Cooperation) (No. 201803D421076 and 201803D421060), Joint Construction Agreement of Shanxi Provincial Key Laboratory for Functional Proteins (No. 213310462-J), China Scholarship Council (No. 201906935015), National Natural Science Foundation of China (No. 51502192).

Appendix A. Supplementary data

Supplementary data to this article can be found online at https://doi.org/10.1016/j.matdes.2022.110711.

References

[1] F.H. Kong, C.H. Fan, Y.L. Yang, et al., 5-hydroxymethylfurfural-embedded poly (vinyl alcohol)/sodium alginate hybrid hydrogels accelerate wound healing, Int. J. Biol. Macromol. 138 (2019) 933–949.
[2] T. Abdelrahman, H. Newton, Wound dressings: principles and practice, Surgery. 29 (10) (2011) 491–495.
[3] R.F. Pereira, C.C. Barrias, P.L. Granja, et al., Advanced biofabrication strategies for skin regeneration and repair, Nanomedicine. 8 (4) (2013) 603–621.
[4] Y. Fan, Q.H. Lu, W.C. Liang, Preparation and characterization of antibacterial polyvinyl alcohol/chitosan sponge and potential applied for wound dressing, Eur. Polym. J. 157 (2021) 110619.
[5] C.C. Maduba, MBBS, FWACS. Split Skin Graft Take in Leg Ulcers: Conventional Dressing Versus Locally Adapted Negative Pressure Dressing, J. Surg. Res. 251 (2020) 296–302.
[6] D. Wang, N.H. Zhang, G.L. Meng, The effect of form of carboxymethyl-chitosan dressings on biological properties in wound healing, Colloids and Surf. B: Biointerfaces., 194 (2020), p. 111191.
[7] G.D. Mogoşanu, A.M. Grumezescu, Natural and synthetic polymers for wounds and burns dressing, Int. J. Pharm. 463 (2) (2014) 127–136.
[8] J. Peng, H. Zhao, C.Z. Tu, In situ hydrogel dressing loaded with heparin and basic fibroblast growth factor for accelerating wound healing in rat, Mater. Sci. Eng., C 116 (2020) 111169.
[9] S. Mehrotra, A. Misir, Special Traumatized Populations: Accidental Hypothermia in Children, Curr. Pediatr. Rev. 14 (1) (2018) 28–33.
[10] D. Simões, S.P. Miguel, M.P. Ribeiro, Recent advances on antimicrobial wound dressing: a review, Eur. J. Pharm. Biopharm. 127 (2018) 130–141.
[11] S.P. Miguel, D.R. Figueira, D. Simes, M.P. Ribeiro, P. Coutinho, P. Ferreira, I.J. Correia, Electrospun polymeric nanofibres as wound dressings: A review, Colloids Surf., B 169 (2018) 60–71.
[12] S.H. Hu, S.C. Bi, D. Yan, Preparation of composite hydroxybutyl chitosan sponge and its role in promoting wound healing, Carbohydrate Polymers Scientific & Technological Aspects of Industrially Important Polysaccharides. 184 (2018) 154–163.
[13] Nakod, Pinaki. The Development of a Textile Wound Dressing for Vacuum Assisted Wound Therapy, 2017.
[14] S. Dhivya, V.V. Padma, E. Santhini, Wound dressings-a review, Biomedicine. 5 (4) (2015) 24–28.
[15] S. Sarabahi, Recent advances in topical wound care, Indian J. Plastic Surg. 45 (2) (2012) 379–387.
[16] P.I. Morgado, A. Aguiar-Ricardo, Asymmetric membranes as ideal wound dressings: An overview on production methods, structure, properties and performance relationship, J. Membr. Sci. 490 (2015) 139–151.
[17] F.L. Mi, Y.B. Wu, S.S. Shyu, A.C. Chao, J.Y. Lai, C.C. Su, Asymmetric chitosan membranes prepared by dry/wet phase separation: a new type of wound dressing for controlled antibacterial release, J. Membr. Sci. 212 (1/2) (2003) 237–254.
[18] S.G. Priya, A. Gupta, E. Jain, J. Sarkar, A. Damania, P.R. Jagdale, Bilayer Cryogel Wound Dressing and Skin Regeneration Grafts for the Treatment of Acute Skin Wounds, ACS Appl. Mater. Interfaces 8 (24) (2016) 15145–15159.
[19] S.P. Miguel, A.F. Moreira, I.J. Correia, Chitosan based-asymmetric membranes for wound healing: A review, Int. J. Biol. Macromol. 127 (2019) 460–475.
[20] H.T. Bui, O.H. Chung, J.D. Cruz, Fabrication and characterization of electrospun curcumin-loaded polycaprolactone-polyethylene glycol nanofibers for enhanced wound healing, Macromol. Res. 22 (12) (2014) 1288–1296.
[21] Y. Ghiyasi, E. Salahi, H. Esfahani, Synergy Effect of Urtica dioica and ZnO NPs on Microstructure, Antibacterial Activity and Cytotoxicity of Electrospun PCL Scaffold for Wound Dressing Application, Mater. Today Commun. 26 (2021) 102163.
[22] A.R. Kakroodi, Y. Kazemi, D. Rodrigue, C.B. Park, Facile production of biodegradable PCL/PLA in situ nanofibrillar composites with unprecedented compatibility between the blend components, Chem. Eng. J. 351 (2018) 976–984.
[23] M.E. Broz, D.L. Vanderhart, N.R. Washburn, Structure and mechanical properties of poly(d, l-lactic acid)/poly(ε-caprolactone) blends, Biomaterials 24 (23) (2003) 4181–4190.
[24] S. Cicero, V. Martínez-Mata, L. Castanon-Jano, Analysis of notch effect in the fracture behaviour of additively manufactured PLA and graphene reinforced PLA, Theor. Appl. Fract. Mech. 114 (2021) 103032.
[25] D. Sharma, D. Saha, B.K. Satapathy, Structurally optimized suture resistant polylactic acid (PLA)/poly (-caprolactone) (PCL) blend based engineered nanofibrous mats – ScienceDirect, J. Mech. Behav. Biomed. Mater. 116 (2021) 104331.
[26] E. Vonbrunn, M. Mueller, M. Pichlsberger, M. Sundl, et al., Electrospun PCL/PLA Scaffolds Are More Suitable Carriers of Placental Mesenchymal Stromal Cells Than Collagen/Elastin Scaffolds and Prevent Wound Contraction in a Mouse Model of Wound Healing, Front Bioeng. Biotechnol. 8 (2020) 604123.
[27] S. Zahid, H. Khalid, F. Ikram, H. Iqbal, M. Samie, L. Shahzadi, A.T. Shah, M. Yar, A. A. Chaudhry, S.J. Awan, A.F. Khan, I.u. Rehman, Bi-layered α-tocopherol acetate loaded membranes for potential wound healing and skin regeneration, Mater. Sci. Eng. C Mater. Biol. Appl. 101 (2019) 438–447.
[28] L. Wang, R.M. Shelton, P.R. Cooper, M. Lawson, J.E. Barralet, Evaluation of sodium alginate for bone marrow cell tissue engineering, Biomaterials 24 (20) (2003) 3475–3481.
[29] R.H. Hirose, N. Watanabe, Y. Naito, Comparison of sodium alginate-based and sodium hyaluronate-based submucosal injection materials based on rheological analysis, J. Mech. Behav. Biomed. Mater. 124 (2021) 104816.
[30] I. Liakos, L. Rizzello, D.J. Scurr, All-natural composite wound dressing films of essential oils encapsulated in sodium alginate with antimicrobial properties – ScienceDirect, Int. J. Pharm. 463 (2) (2014) 137–145.

[31] P.B. Malafaya, G.A. Silva, R.L. Reis, Natural-origin polymers as carriers and scaffolds for biomolecules and cell delivery in tissue engineering applications, Adv. Drug Deliv. Rev. 59 (4–5) (2007) 207–233.
[32] J.M. Seok, S.H. Oh, S.J. Lee, et al., Fabrication and characterization of 3D scaffolds made from blends of sodium alginate and poly(vinyl alcohol), Mater. Today Commun. 19 (2018) 56–61.
[33] T.T. Min, Z. Zhu, X.L. Sun, Z. Yuan, Y. Wen, Highly Efficient Antifogging and Antibacterial Food Packaging Film Fabricated by Novel Quaternary Ammonium Chitosan Composite, Food Chem. 308 (2) (2019) 125682.
[34] N.A. Peppas, E.W. Merrill, Crosslinked poly(vinyl alcohol) hydrogels as swollen elastic networks, J. Appl. Polym. Sci. 21 (7) (2010) 1763–1770.
[35] R. Ricciardi, F. Auriemma, C. Gaillet, C.D. Rosa, F. Lauprêtre, Investigation of the Crystallinity of Freeze/Thaw Poly(vinyl alcohol) Hydrogels by Different Techniques, Macromolecules 37 (25) (2004) 9510–9516.
[36] S.B. Yang, H.Y. Ao, Y. Yang, T. Tang, HACC modified poly (L-Lactic-co-Glycolic Acid) electrospun fibrous scaffold for guided bone regeneration membrane, J. Orthopaedic Translation. 7 (2016) 124–125.
[37] V.R. Ögmundur, J. Holappa, T. Nevalainen, H. Martha, J. Tomi, J.M. Einarsson, Antibacterial activity of methylated chitosan and chitooligomer derivatives: Synthesis and structure activity relationships, Eur. Polym. J. 43 (6) (2007) 2660–2671.
[38] L.L. Qiu, C. Choong, Three-Dimensional Scaffolds for Tissue Engineering Applications: Role of Porosity and Pore Size, Tissue Eng. Part B Rev. 19 (6) (2013) 485–502.
[39] L.L. Ouyang, R. Yao, Y. Zhao, W. Sun, Effect of bioink properties on printability and cell viability for 3D bioplotting of embryonic stem cells, Biofabrication. 8 (3) (2016) 035020.
[40] Q.Q. Liu, Q.T. Li, S. Xu, Q.J. Zheng, Preparation and Properties of 3D Printed Alginate-Chitosan Polyion Complex Hydrogels for Tissue Engineering, Polymers. 16 (6) (2018) 664–675.
[41] Z.M. Dai, D.K. Zhang, K. Chen, Mechanical property analysis of PVA/HA composite hydrogel and its finite element simulation, J. Med. Biomech. 27 (3) (2012) 344–350.
[42] J. Zhou, D.Y. Yao, Z.Y. Qian, S. Hou, Bacteria-responsive intelligent wound dressing: Simultaneous In situ detection and inhibition of bacterial infection for accelerated wound healing, Biomaterials 161 (2018) 11–23.
[43] Q.H. Qiu, S.Y. Chen, Y.P. Li, Functional nanofibers embedded into textiles for durable antibacterial properties, Chem. Eng. J. 384 (C) (2020) 123241.
[44] P.A.J. Kolarsick, M.A. Kolarsick, C. Goodwin, Anatomy and Physiology of the Skin, J. Dermatology Nurses Association. 3 (4) (2011) 203–213.
[45] X.L. Niu, L.F. Wang, M.J. Xu, M. Qin, Electrospun polyamide-6/chitosan nanofibers reinforced nano-hydroxyapatite/polyamide-6 composite bilayered membranes for guided bone regeneration – ScienceDirect, Carbohydr. Polym. 260 (2021) 117769.
[46] M. Chen, P.K. Patra, S.B. Warner, S. Bhowmick, Role of fiber diameter in adhesion and proliferation of NIH 3T3 fibroblast on electrospun poly-caprolactone scaffolds, Tissue Eng. 13 (2007) 579–587.
[47] S.M. Saraiva, S.P. Miguel, M.P. Ribeiro, Synthesis and characterization of a photocrosslinkable chitosan–gelatin hydrogel aimed for tissue regeneration, RSC Adv. 5 (78) (2015) 63478–63488.
[48] S.P. Miguel, M.P. Ribeiro, P. Coutinho, I.P. Correia, Electrospun Polycaprolactone/Aloe Vera_Chitosan Nanofibrous Asymmetric Membranes Aimed for Wound Healing Applications, Polymers. 9 (12) (2017) 183.
[49] R. Scaffaro, F. Lopresti, L. Botta, Preparation, characterization and hydrolytic degradation of PLA/PCL co-mingled nanofibrous mats prepared via dual-jet electrospinning, Eur. Polym. J. 96 (2017) 266–277.
[50] K. Bialik-Wąs, K. Pluta, D. Malina, Advanced SA/PVA-based hydrogel matrices with prolonged release of Aloe vera as promising wound dressings – ScienceDirect, Mater. Sci. Eng., C 120 (2021) 111667.
[51] Y. Zhuang, Y. Kong, K. Han, H. Hao, A physically cross-linked self-healable double-network polymer hydrogel as a framework for nanomaterial, New J. Chem. 41 (24) (2017) 15127–15135.
[52] L. Bacakova, E. Filova, M. Parizek, T. Ruml, V. Svorcik, Modulation of cell adhesion, proliferation and differentiation on materials designed for body implants, Biotechnol. Adv. 29 (6) (2011) 739–767.
[53] S.M. Oliveira, N.M. Alves, J.F. Mano, Cell interactions with superhydrophilic and superhydrophobic surfaces, J. Adhes. Sci. Technol. 28 (8–9) (2014) 843–863.
[54] D.R. Figueira, S.P. Miguel, K.D. Sá, I.J. Correia, Production and characterization of polycaprolactone- hyaluronic acid/chitosan- zein electrospun bilayer nanofibrous membrane for tissue regeneration, Int. J. Biol. Macromol. (2016) 1100–1110.
[55] H. Sliman, X. Dong, T. Zhao, Functionalization of Polyethylene terephthalate Knitted Fabric with cowpea protein and biopolymer complex: Applications for enhancing wettability and UV-Protection Properties, J. Colloid Interface Sci. 565 (2020) 360–367.
[56] M.M. Machado-Paula, M.A.F. Corat, M. Lancellotti, A comparison between electrospinning and rotary-jet spinning to produce PCL fibers with low bacteria colonization – ScienceDirect, Mater. Sci. Eng., C (2020) 110706.
[57] P.T. Kumar, V.K. Lakshmanan, T.V. Anilkumar, C. Ramya, P. Reshmi, R. Jayakumar, Flexible and Microporous Chitosan Hydrogel/Nano ZnO Composite Bandages for Wound Dressing: In Vitro and In Vivo Evaluation, Acs Appl. Mater. Interfaces. 4 (5) (2012) 2618–2629.
[58] F. Martínez-Gómez, J. Guerrero, B. Matsuhiro, J. Pavez, In vitro release of metformin hydrochloride from sodium alginate/polyvinyl alcohol hydrogels, Carbohydr. Polym. 155 (2017) 182–191.
[59] D. Simoes, S.P. Miguel, I.J. Correia, Biofunctionalization of electrospun Poly (caprolactone) fibers with Maillard Reaction Products for wound dressing applications, React. Funct. Polym. 131 (2018) 191–202.
[60] I.R. Serra, R. Fradique, M.C.S. Vallejo, T.R. Correia, Production and characterization of chitosan/gelatin/β-TCP scaffolds for improved bone tissue regeneration, Mater. Sci. Eng., C 55 (2015) 592–604.
[61] S.P. Miguel, C.S.D. Cabral, A.F. Moreira, Production and characterization of a novel asymmetric 3D printed construct aimed for skin tissue regeneration, Colloids Surf., B 181 (2019) 994–1003.
[62] P.I. Morgado, P.F. Lisboa, M.P. Ribeiro, S.P. Miguel, Poly(vinyl alcohol)/chitosan asymmetrical membranes: Highly controlled morphology toward the ideal wound dressing, J. Membr. Sci. 469 (2014) 262–271.
[63] Y.T. Jian, Y. Yang, T. Tian, C. Stanford, Effect of Pore Size and Porosity on the Biomechanical Properties and Cytocompatibility of Porous NiTi Alloys, PLoS ONE 10 (6) (2015) 128138.
[64] H.L. Wang, Y. Zuo, L. Zhang, W.H. Yang, Y.B. Li, Preparation and characterisation of nanohydroxyapatite–sodium alginate–polyvinyl alcohol composite scaffold, Mater. Res. Innovations 14 (5) (2013) 375–380.
[65] D.Q. Gao, X.Q. Zhou, Z.H. Gao, X. Shi, P. Zhang, Preparation and Characterization of Silver Sulfadiazine-Loaded Polyvinyl Alcohol Hydrogels as an Antibacterial Wound Dressing, J. Pharm. Sci. 107 (9) (2018) 2377–2384.
[66] Z.S. Li, H.R. Ramay, K.D. Hauch, D. Xiao, M. Zhang, Chitosan-alginate hybrid scaffolds for bone tissue engineering, Biomaterials 26 (18) (2005) 3919–3928.
[67] 3M™ Tegaderm™ Alginate Ag Silver Dressing, 3M United States https://www.3m.com/3M/en_US/company-us/all-3m-products/~/3M-Tegaderm-Alginate-Ag-Silver-Dressing/?N=5002385+3293321936&rt=rud (2020), Accessed 10th Jul 2020.
[68] Q. Yang, S. Cui, X. Song, et al., An antimicrobial peptide-immobilized nanofiber mat with superior performances than the commercial silver-containing dressing, Mater. Sci. Eng., C 119 (2021) 111608.
[69] M. Schroepfer, F. Junghans, D. Voigt, M. Meyer, I. Prade, Gas-Phase Fluorination on PLA Improves Cell Adhesion and Spreading, ACS Omega 5 (10) (2020) 5498–5507.
[70] L.T.M. Phuc, A. Taniguchi, Polystyrene Nanoparticles Induce Apoptosis or Necrosis With or Without Epidermal Growth Factor, J. Nanosci. Nanotechnol. 19 (8) (2019) 4812–4817.
[71] S.S. Shen, Y.X. Liu, P. Huang, J. Wang, In Vitro Cellular Uptake and Effects of Fe_3O_4 Magnetic Nanoparticles on HeLa Cells, J. Nanosci. Nanotechnol. 9 (5) (2009) 2866–2871.
[72] D. Campoccia, L. Montanaro, C.R. Arciola, The significance of infection related to orthopedic devices and issues of antibiotic resistance, Biomaterials 27 (11) (2006) 2331–2339.
[73] E.L. Tsalik, R.A. Bonomo, V.G. Fowler, New Molecular Diagnostic Approaches to Bacterial Infections and Antibacterial Resistance, Annu. Rev. Med. 69 (2018) 379–394.
[74] T. Tashiro, Antibacterial and Bacterium Adsorbing Macromolecules, Macromol. Mater. Eng. 286 (2) (2001) 63–87.
[75] F.L. Mi, S.S. Shyu, Y.B. Wu, S.T. Lee, R.N. Huang, Fabrication and characterization of a sponge-like asymmetric chitosan membrane as a wound dressing, Biomaterials 22 (2) (2001) 165–173.